INTERNATIONAL JOURNAL FOR NUMERICAL METHODS IN FLUIDS, VOL. 13, 481–489 (1991)

NUMERICAL SOLUTION OF THE NAVIER–STOKES EQUATIONS USING A FINITE ELEMENT METHOD

R. C. MEHTA AND T. JAYACHANDRAN
Vikram Sarabhai Space Centre, Trivandrum 695022, India

AND

V. M. K. SASTRI
Mechanical Engineering Department, Indian Institute of Technology, Madras 600036, India

SUMMARY

A finite element algorithm for solving the Navier–Stokes equations is presented for the analysis of high-speed viscous flows. The algorithm uses triangular elements. The unsteady equations are integrated to steady state with a Runge–Kutta time-marching scheme. A postprocessing artificial dissipation term is introduced to stabilize the computations and to dampen dissipation errors. Numerical results are compared with the calculation of uniform flow on a rectangular region which encounters an embedded oblique shock. A shock/turbulent boundary layer problem is also solved and results are compared with experimental data. It is shown that the postprocessing smoothing term and boundary conditions similar to the finite difference method work well in the present numerical studies.

KEY WORDS Shock/turbulent problem Runge–Kutta time scheme FEM

INTRODUCTION

The techniques for numerical solution of the equations of motion for supersonic flow range from finite volume techniques to finite element techniques for the Navier–Stokes equations. The main difference is that the finite volume method is based on surface integrals whereas the finite element method is based on volume integrals.

Cooke and Blanchard[1] have used a Galerkin technique in conjunction with a predictor–corrector algorithm to solve the Navier–Stokes equations. A Lax–Wendroff type of time marching to get a steady state solution has been developed by Donea.[2] Lohner *et al.*[3] and Thornton *et al.*[4] have solved a variety of flow situations using triangular and quadrilateral elements respectively with a Taylor–Galerkin finite element approach. Hughes *et al.*[5] have applied a Petrov–Galerkin approach for analysing computational fluid dynamics problems. Morgan and Peraire[6] have presented an excellent description of various finite element techniques applied to the numerical solution of compressible flows.

The present paper presents a finite element algorithm for the numerical solution of the Navier–Stokes equations employing Galerkin spatial discretization with triangular elements. A multistage time integration[7] is used in conjunction with the Lapidus artificial dissipation model. The algorithm is used for the numerical calculation in Cartesian co-ordinates of uniform flow on a rectangular region which encounters an embedded shock with known turning angle. The results of

0271–2091/91/140481–09$05.00

Received December 1989
Revised October 1990

the present method are compared with Cooke and Blanchard's[1] solution. A shock/turbulent boundary layer interaction problem is analysed by solving the Navier–Stokes equations with the Cebeci–Smith turbulence model. Boundary conditions similar to the finite difference method are employed in the algorithm. Numerical results are compared with experimental data.[8]

SOLUTION ALGORITHM

The equations solved are the Navier–Stokes equations describing two-dimensional, unsteady and compressible flows. The solution algorithm is applied to the flow equations written in conservative vector form as

$$\frac{\partial \mathbf{U}}{\partial t}+\frac{\partial \mathbf{E}}{\partial x}+\frac{\partial \mathbf{F}}{\partial y}=0. \tag{1}$$

The solution vector **U** and flux vectors **E** and **F** are given by

$$\begin{aligned}\mathbf{U}&=[\rho,\ \rho u,\ \rho v,\ e_T]^T,\\ \mathbf{E}&=[\rho u,\ \rho u^2+p+\tau_{xx},\ \rho uv+\tau_{xy},\ (e_T+p+\tau_{xx})u+\tau_{xy}v-q_x]^T,\\ \mathbf{F}&=[\rho v,\ \rho uv+\tau_{xy},\ \rho v^2+p+\tau_{yy},\ (e_T+p+\tau_{yy})v+\tau_{xy}u-q_y]^T,\end{aligned} \tag{2}$$

where ρ, p and e_T denote the density, pressure and total energy of the fluid respectively, u and v are velocity components in the x- and y-directions respectively, τ_{xx}, τ_{yy} and τ_{xy} are stress components and q_x and q_y are heat fluxes. For a perfect gas the equation set is completed by the addition of the equations of state

$$e_T=\rho I+\tfrac{1}{2}\rho(u^2+v^2), \tag{3a}$$

$$p=(\gamma-1)\rho I, \tag{3b}$$

where I is the internal energy.

Sutherland's law is used to evaluate the molecular viscosity. A two-layer equilibrium eddy viscosity model of Cebeci and Smith[9] is considered in the case of shock/turbulent boundary layer interaction.

Spatial discretization

The domain V is subdivided into triangular finite elements and the approximation $\mathbf{U}^*$ to the solution vector **U** is interpolated using C^0 linear shape functions. A semidiscrete system with time as the only independent variable can be cast by writing the Galerkin weighted residual statement[10]

$$\int_V \left(\frac{\partial \mathbf{U}}{\partial t}+\frac{\partial \mathbf{E}}{\partial x}+\frac{\partial \mathbf{F}}{\partial y}\right) N_i \mathrm{d}V=0, \tag{4}$$

where N_i is the linear finite element shape function associated with node i. The nodal co-ordinates are specified by subdividing the domain V into a number of triangular elements. For a typical triangular element e with nodes numbered anticlockwise as i, j, k and placed at the vertices of the triangle, the shape function N_i^e is

$$N_i^e=a_i^e+b_i^e x+c_i^e y, \tag{5}$$

where

$$a_i^e=\frac{x_j y_k-x_k y_j}{2A^e}, \qquad b_i^e=\frac{y_j-y_k}{2A^e}, \qquad c_i^e=\frac{x_k-x_j}{2A^e},$$

with A^e the area of element e. The Galerkin step can be thought of as a projection onto space spanned by the shape function such that the error is orthogonal to the space.

Inserting linear finite element approximations for **U**, **E** and **F** in equation (4) results in the semidiscrete matrix equations

$$\mathbf{M}\frac{\mathrm{d}U_i}{\mathrm{d}t} = -\int\left(\mathbf{N}^{\mathrm{T}}\frac{\partial \mathbf{N}}{\partial x}E_i + \mathbf{N}^{\mathrm{T}}\frac{\partial \mathbf{N}}{\partial y}F_i\right)\mathrm{d}V, \tag{6}$$

$$\mathbf{M} = \int\int \mathbf{N}^{\mathrm{T}}\mathbf{N}\,\mathrm{d}V, \tag{7}$$

where **N** is the global vector of shape functions (the sum of all elemental shape functions), E_i, F_i and $\mathrm{d}U_i/\mathrm{d}t$ are the nodal values of **E**, **F** and $\partial \mathbf{U}/\partial t$ respectively and **M** is a consistent mass matrix. In the numerical implementation the mass matrix **M** is replaced by the lumped mass matrix $\mathbf{M}_{\mathrm{L}}$ in which each diagonal entry is the sum of all elements in the corresponding row of **M**. This allows equation (6) to be solved explicitly. This does not change the steady state solution but does modify the time stability of the algorithm slightly.

Initial and boundary conditions

Oblique shock flow. The computational domain and triangular grid for the oblique shock calculation are shown in Figure 1. Uniform flow conditions are prescribed on the inflow and prior to the point of occurrence of the shock between nodes A and B on the top boundary including

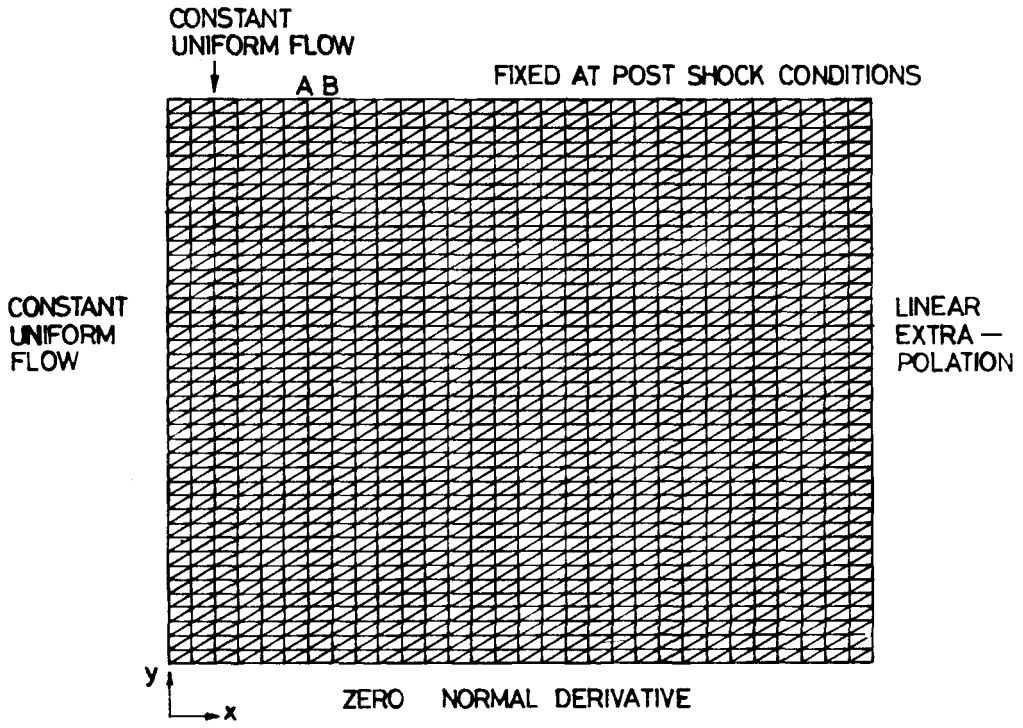

Figure 1. Oblique shock computational domain and grid

point B. Along the remainder of the top boundary, fixed post-shock values corresponding to flow having been turned by a shock at an incidence angle of 23° are prescribed.[1] Computational boundary conditions are applied along the bottom and outflow boundaries: zero normal gradient along the bottom and linear extrapolation on the outflow.

Shock/turbulent boundary layer interaction. This case consists of a supersonic stream at the inflow and outflow boundaries. The initial flow field and boundary conditions are shown schematically in Figure 2. The computational domain is chosen such that the reflected shock wave from the wall does not intersect the top boundaries and the flow is sufficiently well developed after leaving the interaction region. Hence it is appropriate to satisfy all variables at the inflow and top boundaries. The flow variables at the top mesh boundaries were set to either freestream values or values for a given shock strength so that the shock wave would impinge on the plate surface at the lower boundary at a given point. Linear extrapolation from interior points is used for the variables at the outflow. The lower surface was either a plane of symmetry or a wall surface and reflective boundary conditions were employed. The freestream was supersonic, therefore the values at the upstream boundary were held fixed. No slip and isothermal wall conditions are applied at the flat plate. To determine the density along the wall, a commonly used approximation is employed, namely

$$\left.\frac{\partial p}{\partial y}\right|_{\mathrm{w}} = 0 \quad \text{or} \quad p_{\mathrm{w}} = p_{\mathrm{w}+1}. \tag{8}$$

For our present case the first mesh point is close to the wall so this pressure condition is appropriate.[11] The density ρ is then determined from the equation of state (3b).

Time marching

To integrate equation (5), the following multistep time integration scheme[7] is used at time level n:

$$\begin{aligned}
U_i^{(1)} &= U_i^n + \tfrac{1}{4}\lambda(\Delta t_i/M_{Li})R_i(\mathbf{U}^n),\\
U_i^{(2)} &= U_i^n + \tfrac{1}{3}\lambda(\Delta t_i/M_{Li})R_i(\mathbf{U}^{(1)}),\\
U_i^{(3)} &= U_i^n + \tfrac{1}{2}\lambda(\Delta t_i/M_{Li})R_i(\mathbf{U}^{(2)}),\\
U_i^{(4)} &= U_i^n + \lambda(\Delta t_i/M_{Li})R_i(\mathbf{U}^{(3)}),\\
U_i^{n+1} &= U_i^{(4)} + V_i,
\end{aligned} \tag{9}$$

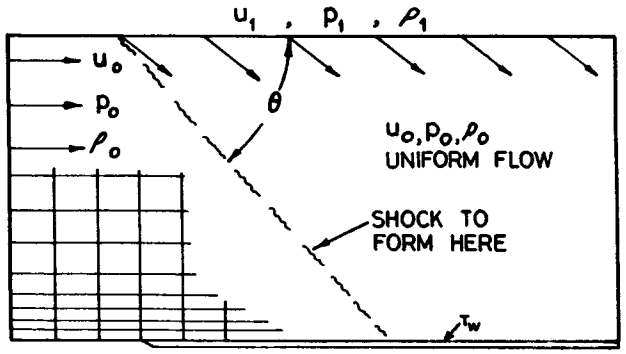

Figure 2. Initial flow field for shock/boundary layer interaction

where $R_i(\mathbf{U})$ is the right-hand side of equation (5) with fluxes based on the state vector $\mathbf{U}$, V_i is a smoothing term and λ is the CFL number. For a time-marching scheme λ must be less than $2\sqrt{2}$. Local time stepping is used to accelerate convergence to steady state. The boundary conditions are satisfied pointwise in a postprocessing procedure.

Smoothing

To prevent oscillations in the vicinity of a discontinuity, the computed $\mathbf{U}^{n+1}$ needs to be smoothed before proceeding to the next step. An artificial dissipation form due to Lapidus[12] is convenient to implement because it uses variables easily computed from conservation variables. The viscous flux components $\mathbf{E}_v$ and $\mathbf{F}_v$ are used in the following form:

$$\left(\frac{\partial \mathbf{E}_v}{\partial x}+\frac{\partial \mathbf{F}_v}{\partial y}\right)_v=\frac{\partial}{\partial x}\left(\kappa A_e\left|\frac{\partial u}{\partial x}\right|\frac{\partial \mathbf{U}}{\partial x}\right)+\frac{\partial}{\partial y}\left(\kappa A_e\left|\frac{\partial v}{\partial y}\right|\frac{\partial \mathbf{U}}{\partial y}\right), \tag{10}$$

where κ is an adjustable dissipation parameter and A_e is the element area.

NUMERICAL PROCEDURE AND RESULTS

Oblique shock flow

A test case of oblique shock flow is considered to validate the algorithm. Table I gives the test conditions used to simulate the introduction of the shock between grid points on the upper boundary. The computations were performed on a CDC CYBER 170/730 digital computer. A uniform 41×31 grid is chosen for computational purposes as depicted in Figure 1. A Prandtl number $Pr = 0{\cdot}72$, Reynolds number $Re = 80{,}869$ and freestream Mach number $M = 3{\cdot}0$ are used in the flow simulations. The criterion for convergence of calculation used herein is

$$|\rho_{n+1}-\rho_n| \leqslant 10^{-4},$$

where n is the iteration index. The density ratio across the shock and the streamwise and normal velocity profiles are given in Figures 3(a)–(c) respectively. The pressure contours over the computational domain are displayed in Figure 4.

By drawing a straight line at 23° angle of incidence and intersecting the top boundary at $x = 0{\cdot}1667$, the interaction of this line with the grid lines $x = x_i$ should yield a y-value in close proximity to the theoretical shock jump location. The horizontal lines in Figure 3(a), in which the density ratio across the shock is plotted, indicate this location. The calculations of the present analysis exhibit good agreement with the numerical results of Cooke and Blanchard[1] and also with the theoretical shock jump location.

Table I. Conditions for oblique shock simulation

Uniform flow conditions	Post-shock conditions
$M = 3{\cdot}0$	2·75799
$\rho = 1{\cdot}0$	1·29341
$u = 1{\cdot}0$	0·96537
$v = 0{\cdot}0$	−0·08159
$T = 0{\cdot}19841$	0·22034

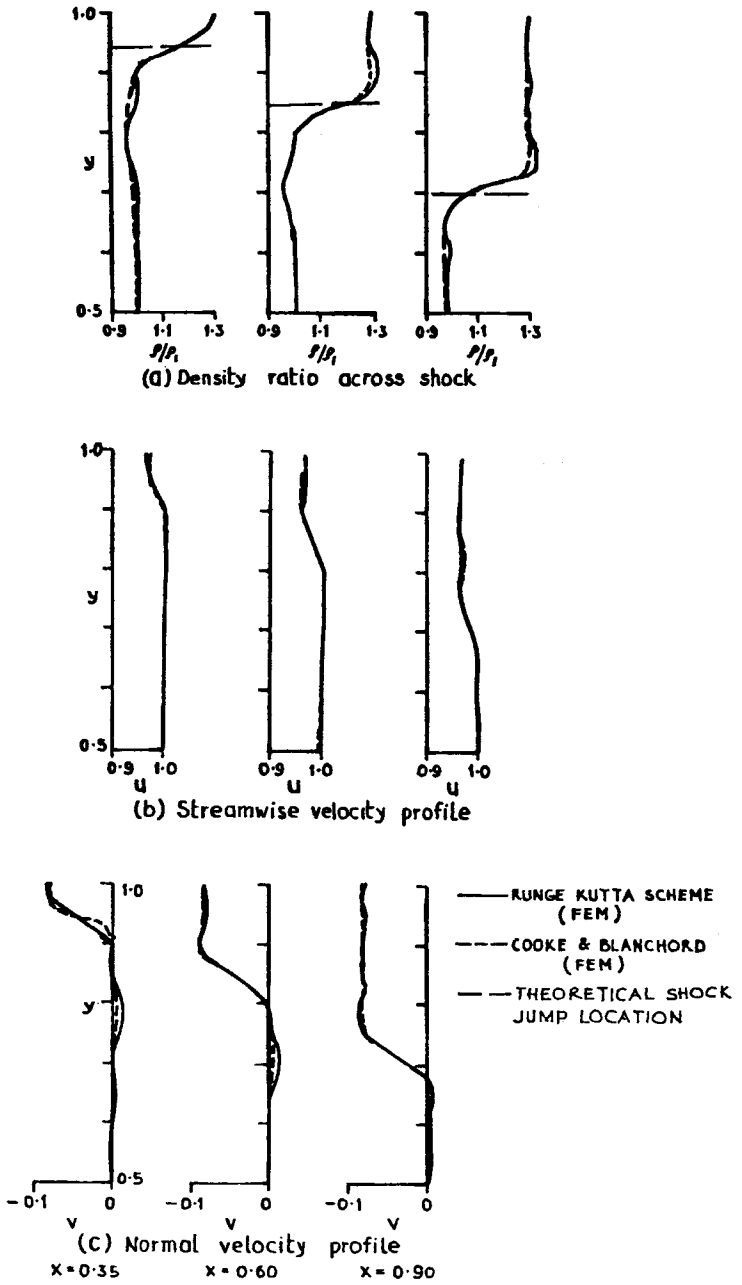

Figure 3. Oblique shock FEM computational results

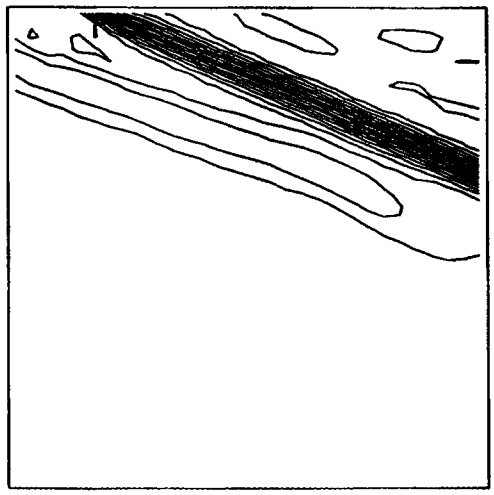

Figure 4. Oblique shock pressure contours

Shock/turbulent boundary layer interaction

The Reynolds-averaged Navier–Stokes equations (1) are solved using a Galerkin–Runge–Kutta procedure. The impinging planar shock strikes the flat plate at an angle of 23° at a freestream Mach number $M = 3{\cdot}7$, Reynolds number $Re/\mathrm{m} = 8{\cdot}202 \times 10^6$ and a wall-to-stagnation temperature ratio $T_W/T_H = 0{\cdot}45$. The total number of grid points is 42×42 and approximately 50% of the mesh points are spanned by the boundary layer. The computational mesh consists of a fine mesh, exponentially stretched inner region in order to increase the concentration of grid points near the wall, and a coarse uniform outer mesh. The present computation was performed on a CDC CYBER 170/730 digital computer for which 131K memory was made available to the user. The convergence criterion required to obtain a steady state solution was considered as mentioned above. This convergence criterion is achieved in approximately 2 h of computer time.

Distributions of the disturbed pressure and heat transfer coefficient normalized by undisturbed quantities, (P_2/P_1 and h_2/h_1), are given in Figures 5 and 6 respectively. The comparisons of the computational results with the experimental data of Back and Cuffel[8] show good agreement. The capability of the algorithm has thus been demonstrated; however, room for improvement still exists.

CONCLUSIONS

A finite element procedure using triangular elements with a multistep Galerkin–Runge–Kutta time-marching algorithm has been used to model shock/turbulent boundary layer interaction flows. A postprocessing smoothing term and boundary conditions similar to the finite difference method are used in the algorithm. The disturbed pressure and heat transfer coefficient show good agreement with the experimental data of Back and Cuffel.[8] The procedure indicates good potential for aerothermal load prediction in the design of high-speed vehicles.

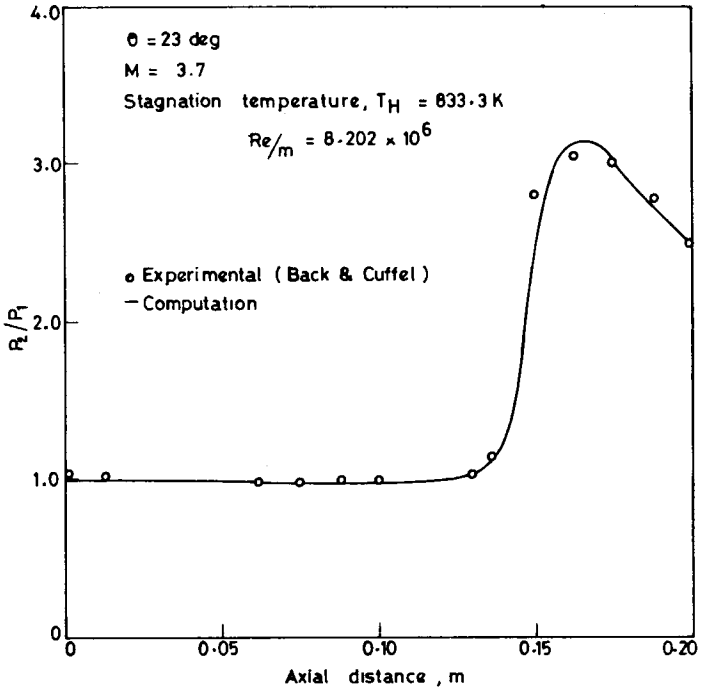

Figure 5. Comparison of computed and measured surface pressure distributions

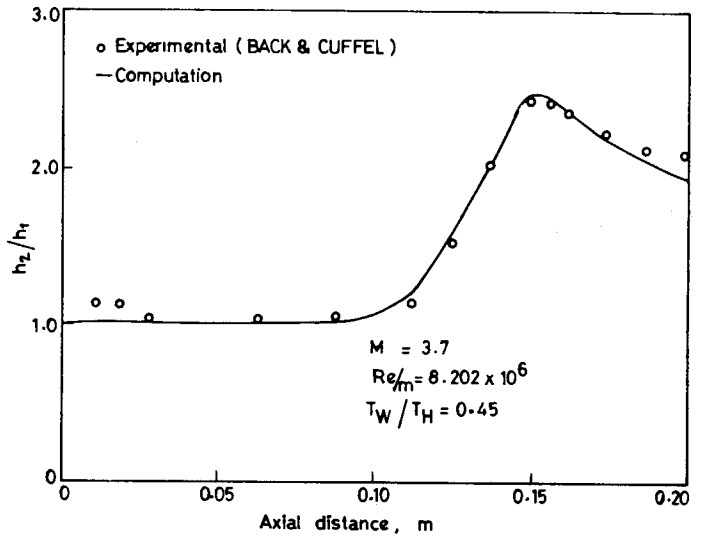

Figure 6. Comparison of computed and measured heat transfer coefficients on the surface

REFERENCES

1. C. H. Cooke and D. K. Blanchard, 'A shock capturing application of the finite element method', *Int. j. numer. methods eng.*, **14**, 271–286 (1979).
2. J. Donea, 'A Taylor–Galerkin method for convective transport problem', *Int. j. numer. methods eng.*, **20**, 101–119 (1984).
3. R. Lohner, K. Morgan and O. C. Zienkiewicz, 'The solution of nonlinear hyperbolic equation systems by the finite element method', *Int. j. numer. methods fluids*, **4**, 1043–1063 (1984).
4. E. A. Thornton, P. Dechaumphai and G. Vemaganti, 'A finite element approach for prediction of aerothermal loads', *AIAA Paper 86-1050, 4th Fluid Mechanics, Plasma Dynamics and Lasers Conf.*, Atlanta, GA, 1986.
5. T. J. R. Hughes, M. Mallet and L. P. Franca, 'New finite element methods for the compressible Euler and Navier–Stokes equations', *7th Int. Conf. on Computing Methods in Applied Sciences and Engineering*, Versailles, France, 1985.
6. K. Morgan and J. Peraire, 'Finite element methods for compressible flows', *Von Karman Institute for Fluid Dynamics, Lecture Series 1987-04*, March 1987.
7. A. Jameson, W. Schmidt and E. Turkel, 'Numerical solution of Euler equations by finite volume methods using Runge–Kutta time-stepping schemes, *AIAA Paper 81-1259*, 1981.
8. L. H. Back and R. F. Cuffel, 'Changes in heat transfer from turbulent boundary layers interacting with shock waves and expansion waves', *AIAA J.*, **8**, 1871–1873 (1970).
9. T. Cebeci, 'Calculation of compressible turbulent boundary layers with heat and mass transfer', *AIAA J.*, **9**, 1091–1097 (1971).
10. O. C. Zienkiewicz and K. Morgan, *Finite Elements and Approximations*, Wiley, New York, 1983.
11. C. M. Hung, 'Numerical solution of supersonic laminar flow over an inclined body of revolution', *AIAA Paper 79-1547*, 1979.
12. R. Lohner, K. Morgan, J. Peraire and O. C. Zienkiewicz, 'Finite element methods for high speed flows', *AIAA Paper 85-1531 CP*, 1985.